THE JOURNAL OF BIOLOGICAL CHEMISTRY
Vol. 280, No. 17, Issue of April 29, pp. 17363–17370, 2005
Printed in U.S.A.

Structural Investigation of *Borrelia burgdorferi* OspB, a BactericidalFab Target*

Received for publication, November 12, 2004, and in revised form, February 11, 2005
Published, JBC Papers in Press, February 15, 2005, DOI 10.1074/jbc.M412842200

Michael Becker‡§, Jonas Bunikis¶, Barbara D. Lade‡, John J. Dunn‡, Alan G. Barbour¶, and Catherine L. Lawson‖****

From the ‡Biology Department, Brookhaven National Laboratory, Upton, New York 11973, the ¶Departments of Microbiology & Molecular Genetics and Medicine, University of California at Irvine, College of Medicine, Irvine, California 92697, and the ‖Department of Chemistry and Chemical Biology, Rutgers University, Piscataway, New Jersey 08854

Certain antibody Fab fragments directed against the C terminus of outer surface protein B (OspB), a major lipoprotein of the Lyme disease spirochete, *Borrelia burgdorferi*, have the unusual property of being bactericidal even in the absence of complement. We report here x-ray crystal structures of a C-terminal fragment of *B. burgdorferi* OspB, which spans residues 152–296, alone at 2.0-Å resolution, and in a complex with the bactericidal Fab H6831 at 2.6-Å resolution. The H6831 epitope is topologically analogous to the LA-2 epitope of OspA and is centered around OspB Lys-253, a residue essential for H6831 recognition. A β-sheet present in the free OspB fragment is either disordered or removed by proteolysis in the H6831-bound complex. Other conformational changes between free and H6831-bound structures are minor and appear to be related to this loss. In both crystal structures, OspB C-terminal fragments form artificial dimers connected by intermolecular β-sheets. OspB structure, stability, and possible mechanisms of killing by H6831 and other bactericidal Fabs are discussed in light of the structural data.

Lyme disease is a serious disease of the skin, joints, nervous system, and heart caused by the spirochete, *Borrelia burgdorferi* (1). In the Eastern United States, the disease is transmitted to humans by the bite of the deer tick, *Ixodes scapularis*. Related spirochetes also cause Lyme disease, including *Borrelia garinii* and *Borrelia afzelii* in Europe and in Asia.

Outer surface proteins A and B (Osp[1]A and OspB) are basic lipoproteins encoded by a single operon located on a 54-kb linear plasmid of the *B. burgdorferi* genome (2, 3). Both are abundant in cultured organisms. OspB (31 kDa, apparent size 34 kDa by SDS-PAGE) has 53% sequence identity to OspA (28 kDa, apparent size 31 kDa by SDS-PAGE). The N termini of both proteins are lipidated following signal peptide cleavage (4). The structure of a recombinant, nonlipidated OspA has been determined in complexes with antigen-binding fragments (Fabs) of two different murine monoclonal antibodies (5–7). Both OspA and OspB are expressed by *B. burgdorferi* in infected unfed ticks, but are down-regulated during tick feeding (8–10). Recent studies suggest that both lipoproteins may play a role in *B. burgdorferi* colonization and survival within the tick (11). OspA and OspB may also be expressed in late stage human disease (12).

Within each *Borrelia* species, OspA is largely invariant in amino acid sequence and antigenic reactivity, but OspB varies significantly (13–16). Probably for this reason, even though both OspA and OspB induce protective immunity in mice (17–19), only OspA has been developed as a protective vaccine against Lyme borreliosis (20, 21). Primary isolates of *B. burgdorferi* vary widely in reactivity of full-length OspB with specific anti-OspB monoclonal antibodies (mAbs) (13), and C-terminally truncated forms of OspB (apparent molecular mass, 18–21.5 kDa) are common (22–24).

Protective antibodies raised against OspA or OspB are generally directed toward the lipoprotein C terminus (7, 22, 25–27). Antibody-mediated bacterial lysis normally involves recruitment of the complement cascade through the constant (Fc) portion of multiple antibody molecules bound to the bacterial surface (28). However, antibodies directed against OspA or OspB do not always require complement to kill *B. burgdorferi* (29). In particular, two independently characterized protective IgG class mAbs directed to the OspB C terminus, H6831 and CB2, have been shown to kill spirochetes in the absence of phagocytes and without complement (30–32). For these mAbs, monovalent antigen binding fragments (Fabs) produced by proteolytic cleavage of whole IgG will also cause lysis (30–32). This unusual phenomenon has also been observed for mAbs against several other spirochete surface proteins (29, 30, 33–35).

The mechanism of complement-independent killing by these antibodies is not known. To examine whether bactericidal action could involve distinctive features of the antibody or defined structural changes in the target antigen, we set out to investigate the structure of OspB in the presence and absence of a bactericidal Fab. Because full-length recombinant, unlipidated OspB (*B. burgdorferi* strain B31) is vulnerable to proteolytic

* This work was supported by National Institutes of Health Grant R01-A137256 (to J. J. D. and C. L. L.), and by National Institutes of Health Grants AI37248 and AI24424 (to A. G. B.). The costs of publication of this article were defrayed in part by the payment of page charges. This article must therefore be hereby marked "*advertisement*" in accordance with 18 U.S.C. Section 1734 solely to indicate this fact.

The atomic coordinates and structure factors (code 1P4P and 1RJL) have been deposited in the Protein Data Bank, Research Collaboratory for Structural Bioinformatics, Rutgers University, New Brunswick, NJ (http://www.rcsb.org/).

§ To whom correspondence may be addressed: Biology Dept., Bldg. 463, Brookhaven National Laboratory, P.O. Box 5000, Upton, NY 11973. Tel.: 631-344-4739; Fax: 631-344-3407; E-mail: mbecker@bnl.gov.

** To whom correspondence may be addressed: Dept. of Chemistry & Chemical Biology, Rutgers University, 610 Taylor Rd., Piscataway, NJ 08854. Tel.: 732-445-8074; Fax: 732-445-5312; E-mail: cathy.lawson@rutgers.edu.

[1] The abbreviations used are: Osp, outer surface protein; CT, C terminus; mAb, monoclonal antibody; PEG, polyethylene glycol; PEG550MME, polyethylene glycol 550 monomethyl ether; r.m.s., root mean square; MOPS, 4-morpholinepropanesulfonic acid; PDB, Protein Data Bank; Bicine, *N*,*N*-bis(2-hydroxyethyl)glycine.

TABLE I
Crystal data and x-ray diffraction statistics

Crystal form	OspB-CT	OspB-CT+H6831 Fab
Space group	$C222_1$	C2
Unit cell dimensions	a = 30.8 Å	a = 186.3 Å
	b = 51.7 Å	b = 37.3 Å
	c = 158.8 Å	c = 87.9 Å
		β = 90.7°
Asymmetric unit	1 OspB-CT fragment	1 OspB-CT/Fab complex
V_M (Å^3/Da) solvent content	2.03	2.06 (see text)
	39.4%	52.4%
Data collection temperature (K)	283	288
No. of crystals	1	3
Wavelength (Å)	0.979, 1.073	0.98
Resolution range (last shell) (Å)	50–2.00 (2.03–2.00)	50–2.60 (2.64–2.60)
No. reflections measured	213,479	139,832
No. unique reflections	9,012	19,155
$\langle I/\sigma \rangle$	34.1 (12.6)	14.6 (4.8)
Completeness (%)	90.2 (77.9)	94.3 (87.6)
*R*merge (%)	6.3 (20.5)	7.8 (15.7)

degradation,[2] we generated a 16.5-kDa C-terminal domain fragment containing the bactericidal Fab-binding epitope (OspB-CT), beginning approximately in the predicted center of the central β-sheet domain (residues 152–296). Crystals of OspB-CT alone and in complex with H6831 Fab were obtained, and their structures were determined. In the H6831-bound structure, four β-strands corresponding to the central β-sheet are either disordered or removed by proteolysis, and additional minor conformational changes are observed. The structural changes appear to result only indirectly from addition of Fab. We discuss the implications of the structural results on OspB fold, stability, and the unusual bactericidal effect.

MATERIALS AND METHODS

Gene Construction, Expression, Purification, and Sequencing—A gene construct encoding the C-terminal fragment of OspB was produced by PCR amplification of *B. burgdorferi* DNA using the following two primers: 5′-CCGG**GATCCATATG**GCTAATAAATTAGACTCA-3′ (forward) and 5′-CCGATATC**GGATCC**TTATTTTAAGGCGTTTTTAA-GC-3′ (reverse).

Regions that overlap the *ospB* gene sequence beginning at amino acid residue 152 and ending at the TAA stop codon after residue 296 are underlined. These primers incorporate NdeI and BamHI restriction sites (bold), permitting cloning into the corresponding sites of the T7-based pET9c expression vector (68). This construction was cloned into *Escherichia coli* DH5α. DNA sequencing revealed that no unwanted mutations were introduced during amplification and cloning. The construct was then transferred to *E. coli* BL21(DE3)/pLysS for T7-RNA polymerase-based protein expression. Cells (500 ml) were grown to mid-logarithmic phase at 310 K in M9TBYG medium supplemented with 50 μg/ml kanamycin, then were induced with 0.5 mM isopropyl-1-thio-β-D-galactopyranoside, and cultured for an additional 3 h. Cells were harvested by centrifugation (15,000 $\times$ *g* at 277 K for 10 min) and then suspended in 25 ml of 20 mM sodium phosphate, 10 mM sodium chloride, pH 7.7 (buffer A). After addition of phenylmethylsulfonyl fluoride to 0.5 mM, leupeptin to 0.4 mM and bacitracin to 0.1 μg/ml, the cells were lysed with three cycles of freezing and thawing. DNase (5 μg/ml of lysate) and magnesium chloride (2.5 mM) were added. The lysate was allowed to remain on ice for 30 min and then centrifuged at 30,000 $\times$ *g* for 20 min at 277 K. The supernatant was passed through a 5-ml Econo-Pac® High Q cartridge (Bio-Rad) equilibrated with buffer A. OspB-CT was recovered in the flow-through and then dialyzed overnight against 500 ml of 10 mM sodium phosphate, pH 6.0 (buffer B) containing 5 mM sodium chloride at 277 K. The dialyzed sample was clarified by brief centrifugation and then applied to a 5-ml Econo-Pac® High S cartridge equilibrated with buffer B. OspB-CT was eluted with application of a gradient of sodium chloride from 0–100 mM. Peak fractions eluting at 60 mM sodium chloride were pooled and concentrated by pressure filtration using a 10-kDa membrane (Amicon) to ~15 mg/ml. The final yield was ~75 mg.

H6831 was purified from the hybridoma supernatant, and Fabs were produced using commercial kits (Pierce) as described (30) and stored at 253 K. The OspB-CT·H6831 complex was formed by incubating freshly prepared OspB-CT with H6831 Fab for about 1 h at 277 K, with OspB-CT in a slight molar excess. The mixture was concentrated in a 20-kDa cutoff Centricon unit (Amicon). This procedure also removed excess OspB-CT. The final concentration was ~6 mg/ml.

Amino acid sequences for the complete light chain and the heavy chain variable domain of mAb H6831 (murine IgG2A, kappa) were determined by using reverse transcriptase to produce cDNAs, followed by PCR to amplify the cDNAs. The amplified cDNAs were then cloned, and the inserts were sequenced using custom primers. The constant region IgG2A heavy chain sequence was taken from Kabat entry 013570.

Crystallization and X-ray Diffraction—Crystallization was by the hanging-drop vapor-phase diffusion method, using Linbro plates. Initial screens were performed with Hampton Research crystallization kits Crystal Screen I and II at 277 and 295 K. Systematic variation of initial screen recipes yielded the three crystal forms reported here. pH values were determined after mixing of the crystallization solutions, prior to mixing with protein. PEG550MME was obtained from Fluka; PEG 3350 was from J. T. Baker; propionamide was from Aldrich. Cryocooling was not attempted, as the OspB-CT crystal form proved very stable in the beam and as crystals of the complex were rare and took a long time to grow.

The OspB-CT crystal form was obtained by mixing 4 μl of freshly purified protein with 4 μl of 25% PEG550MME, 0.1 M Bicine, 0.1 M sodium bromide, 0.03 M sodium citrate, pH 9.5, and equilibrating at 295 K against 1 ml of the same crystallization solution. Long needles reached sizes of up to 1.2 mm $\times$ 0.4 mm $\times$ 0.1 mm in about 2 weeks. X-ray diffraction data were collected from a single crystal mounted in a 0.7-mm diameter glass capillary and cooled to 283 K at beamline X12-B of the NSLS. Diffraction was observed to at least 1.6-Å resolution, and complete data were collected to a 2.0-Å resolution limit (Table I).

Crystals of the OspB-CT + H6831 Fab complex were obtained by mixing 4 μl of complex with 4 μl of either: (*a*) 25% PEG 3350, 0.2 M sodium citrate, pH 5.6, (*b*) 25% PEG 3350, 5% isopropyl alcohol, 0.2 M sodium citrate, pH 5.6, or (*c*) 25% PEG 3350, 5% propionamide, 0.1 M MOPS, 0.2 M ammonium sulfate, pH 7.5, and then equilibrated against a 1-ml reservoir of the same solution. Crystals were rare and slow to form, appearing after several months of incubation at 277 K, with dimensions of up to 0.4 mm $\times$ 0.3 mm $\times$ 0.1 mm. Crystals were mounted in thin-walled glass capillaries, and native diffraction data were collected with cooling to 288 K. Diffraction data (Table I) could be merged satisfactorily from three crystals, one each from conditions (*a*), (*b*), and (*c*).

Diffraction data were collected on beamlines X12B and X12C of the National Synchrotron Light Source (NSLS). All data were processed using Denzo and Scalepack (69).

Structure Determination and Analysis—The structure of OspB-CT was determined by molecular replacement, using the C-terminal-half of OspA as a search model (PDB ID 1OSP, Ref. 6, residues 134–273). The rotation function was performed with AMORE (70). Patterson correlation refinement of the rotation solution was performed with CNS (71), followed by determination of the translation function with a modified version of Merlot (72). The model was refined with CNS using simulated annealing and conjugate-gradient minimization against the maximum likelihood function. Model adjustments were performed with Turbo-

[2] B. D. Lade and J. J. Dunn, unpublished results.

TABLE II
Model statistics

Crystal form	OspB-CT	OspB-CT + H6831 Fab
R_{work}	0.211	0.191
R_{free}	0.260	0.235
Average B (Å^2), all atoms	32.3	39.2[a]
R.m.s. bonds (Å)	0.015	0.006
R.m.s. angles (°)	1.6	1.7
No. protein residues	140	533
No. waters	118	144
PDB ID	1P4P	1RJL

[a] Average B (Å^2), all atoms, Fab alone is 34.7; average B (Å^2), all atoms, OspB-CT (res. 202–296) is 58.3.

Frodo, guided by composite omit maps and sigma-weighted $2F_o$-F_c maps. Refmac (73) was used for the final stages of refinement. No cutoff in F was used in the refinement. Final model statistics are shown in Table II. PROCHECK (74) yields 85.9, 10.9, 2.3, and 0.8% in most favored, allowed, generously allowed, and disallowed regions of the Ramachandran plot, respectively. The density for Asp-251, which is in a generously allowed region, is well defined. The remaining residues in the generously allowed and disallowed regions (Glu-217, Lys-218, and Lys-221) are part of a loop with poorly defined electron density.

The structure of the complex was determined by molecular replacement with AMORE. The location of the Fab was readily determined using the structure of anti-OspA Fab 184.1 (PDB ID 1OSP) (6) as the search model, with non-conserved residues truncated to alanine, but a satisfactory molecular replacement solution for OspB-CT was not obtained. The partial phases provided by the Fab solution yielded a difference electron density for the OspB-CT molecule in the position of the antigen recognition site. The three OspB-CT loops contacted by the Fab were identified using a ridgeline representation of the difference map. It was then possible to fit OspB-CT residues 202–296 into the remaining difference density. An additional 5-residue poly(Ala) strand that passes through a crystallographic 2-fold symmetry axis was modeled at 50% occupancy (see "Results"). Refinement was performed with CNS. No cutoff in F was used in the refinement. The final model statistics are shown in Table II. PROCHECK yields 84.4, 14.5, 1.1, and 0.0% in most favored, allowed, generously allowed, and disallowed regions of a Ramachandran plot, respectively. Residues Cys-135 and Asp-137 of the Fab H-chain and Lys-218 of OspB-CT in the complex are in generously allowed regions; in each case electron density is poorly defined. Electron density for Thr-262 of OspB-CT is also poorly defined.

Accessible surface calculations were performed with CNS. Cavity calculations were performed using GRASP (36). Molecular graphics images were prepared with Setor (75) and Pymol (www.pymol.org).

RESULTS

Crystal Structure of OspB-CT—The structure of OspB-CT was determined to a resolution of 2.0 Å. The model extends from Ser-157 to Lys-296; N-terminal residues 152–156 were not visible in electron density. As expected from sequence similarity, OspB-CT adopts the same fold as is observed for the C-terminal-half of OspA (compare Fig. 1*a* with Fig. 2*a*). The OspB-CT structure consists of twelve anti-parallel β-strands followed by a single α-helix. OspB-CT β-strands 1–4 form a free-standing sheet at the artificial N terminus that is equivalent to the C-terminal four strands of the OspA eight-stranded central sheet (OspA β-strands 10–13). OspB-CT β-strands 5–12 form two additional sheets that together with the C-terminal α-helix fold into a barrel-like domain. Superposition of 138 equivalent main chain C_α atoms of OspB-CT onto OspA yields an r.m.s. deviation of only 1.65 Å.

In the OspA structure, Li *et al.* (6) identified a potential binding site for an unknown ligand consisting of three charged residues contributed by three separate β-strands: Arg-139, Glu-160, and Lys-189. These residues are partially buried at the base of a prominent cleft about 5-Å wide, 24-Å long, and 8-Å deep. The side chain of Lys-189 forms a lid on a hydrophobic cavity of about 34 Å^3. A similar charge triad is formed in OspB-CT by the residues Arg-162, Glu-184, and Arg-214 (Fig. 1*b*), and is situated at the base of an analogous prominent cleft. The side chain of Arg-214 forms the lid on an analogous cavity

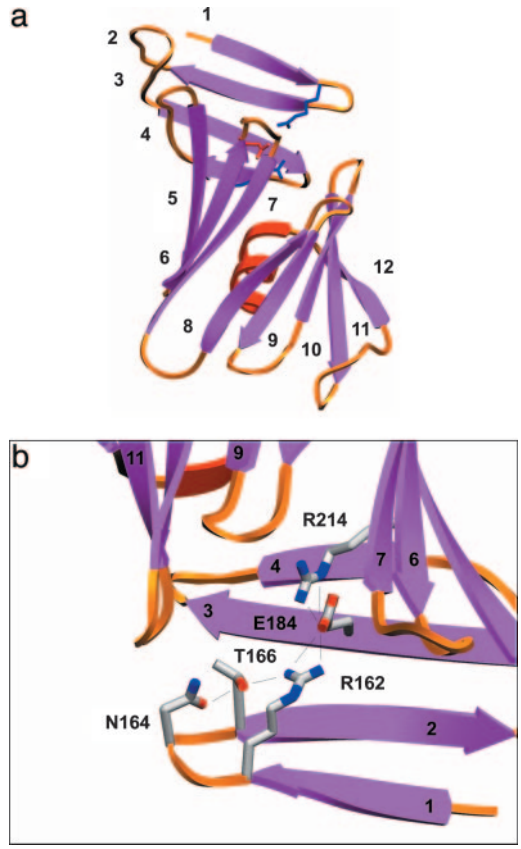

FIG. 1. *a*, *ribbon diagram* of OspB-CT, with strand numbers labeled. The side chains of charge triad residues Arg-162 (*blue*), Glu-184 (*red*), and Arg-214 (*blue*) are also indicated. *b*, close-up of charge triad region. View is upside down relative to *panel a*. Side chains of Arg-162, Glu-184, Arg-214, and nearby residues Thr-166, Asn-164 are shown with atom-colors (oxygen, *red*; nitrogen, *blue*). Predicted hydrogen bonds (distance ≤ 3.2 Å) are indicated by *thin lines*.

of about 35 Å^3. No density is observed within the cavity of either OspA or OspB-CT.

In the crystal, OspB-CT dimerizes with perfect 2-fold symmetry through anti-parallel association of N-terminal OspB-CT strands (Fig. 2*b*). The same symmetric dimer is also present in a second crystal form of OspB-CT (data not shown). The intermolecular 8-stranded "free-standing" β-sheet possessed by the OspB-CT dimer is analogous to the intramolecular free-standing β-sheet found in OspA (compare Fig. 2, *a* and *b*). Two lysine residues are brought into close proximity at the dimer interface. The relatively high pH of crystallization (9.5) probably mitigates unfavorable charge interactions between these residues. In addition, each lysine appears to be stabilized by charge-polar or charge-charge interactions with glutamates on adjacent strands.

Crystal Structure of an OspB-CT·Bactericidal Fab Complex—The structure of the OspB-CT·H6831Fab complex was determined to 2.6-Å resolution. The final refined model includes OspB-CT residues 202–296 plus Fab heavy and light chains; OspB-CT residues 157–201 were not visible in electron density. The structure reveals that three adjacent surface-exposed loops of OspB-CT are contacted by the Fab (Fig. 3*a*). The H6831 epitope of OspB is topologically equivalent to the LA-2 epitope of OspA (7) (Fig. 3*b*). A striking feature of the OspB-CT·H6831 interaction is the prevalence of aromatic residues contributed by the Fab (Fig. 3*c*), a feature common to antigen-antibody complexes (37). The majority of electrostatic and hydrogen-bonded interactions are between loop 2 (residues 250–254) and the Fab heavy chain; these include one ion pair,

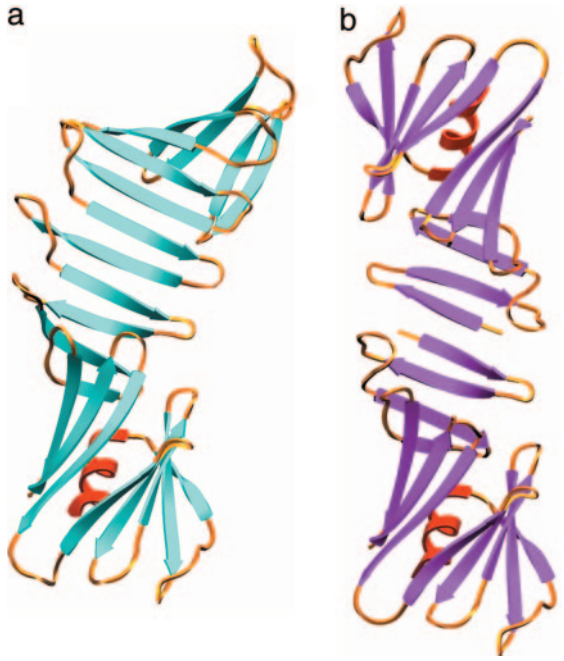

FIG. 2. *a*, *ribbon diagram* of OspA (PDB ID 1OSP, chain A, Ref. 6). *b*, *ribbon diagram* of the crystallographic OspB-CT dimer in the same orientation.

three direct hydrogen bonds, and one water-mediated hydrogen bond. There are two hydrogen bonds between loop 1 (residues 231–233) and the Fab heavy chain, and two hydrogen bonds between loop 3 (residues 272–276) and the Fab light chain. Three waters form well defined hydrogen-bonded bridges between the heavy and light chains of the Fab across the antigen-combining site. There are only small conformational differences in the epitope loops in the complex compared with free OspB-CT (more details given below). The buried surface area at the interface of the OspB-CT·H6831 complex (1095 Å^2) is smaller than that buried at the interface of the OspA·LA2 complex (1599 Å^2). In the case of the OspA·LA-2 complex, loop 1 has the most extensive interactions with the Fab, whereas in the case of OspB-CT·H6831 complex, loop 1 has the fewest interactions with the Fab (Fig. 4*a*, *bar graph*).

Full-length OspBs that fail to bind anti-OspB bactericidal Fabs H6831 or CB2 have amino acid substitutions at position 253 that replace lysine with a different residue (30, 32). Lys-253 is situated on loop 2 and in the free OspB-CT structure it is solvent-exposed with poorly defined side chain electron density. In the complex structure, the electron density is well defined, and there is extensive contact between Lys-253 and the antigen-combining site of the Fab (Fig. 3*c*). The Lys-253 side chain adopts an all-*trans* conformation and is wedged between two aromatic residues of the Fab: a tyrosine and a tryptophan. In addition, the Lys-253 primary amine makes a hydrogen bond/ion pair with a glutamate from the Fab heavy chain, a second hydrogen bond with a main chain carbonyl from loop 1 of OspB-CT, and a water-mediated hydrogen bond to a histidine from the Fab heavy chain. Direct contacts between OspB-CT and the Fab are mediated entirely through residues of the three loops (Fig. 4*a*, *bars*). The two OspB residues that contribute most to the interface are Lys-253 (93 Å^2) and Thr-276 (87 Å^2).

The OspB-CT·H6831 complex crystal also features an artificial OspB-CT dimer (Fig. 5*a*), but the interface is distinct from that observed in the free OspB-CT structure. The most N-terminal residue of OspB-CT for which there is well connected electron density is Thr-202 at the start of β-strand 5, the first

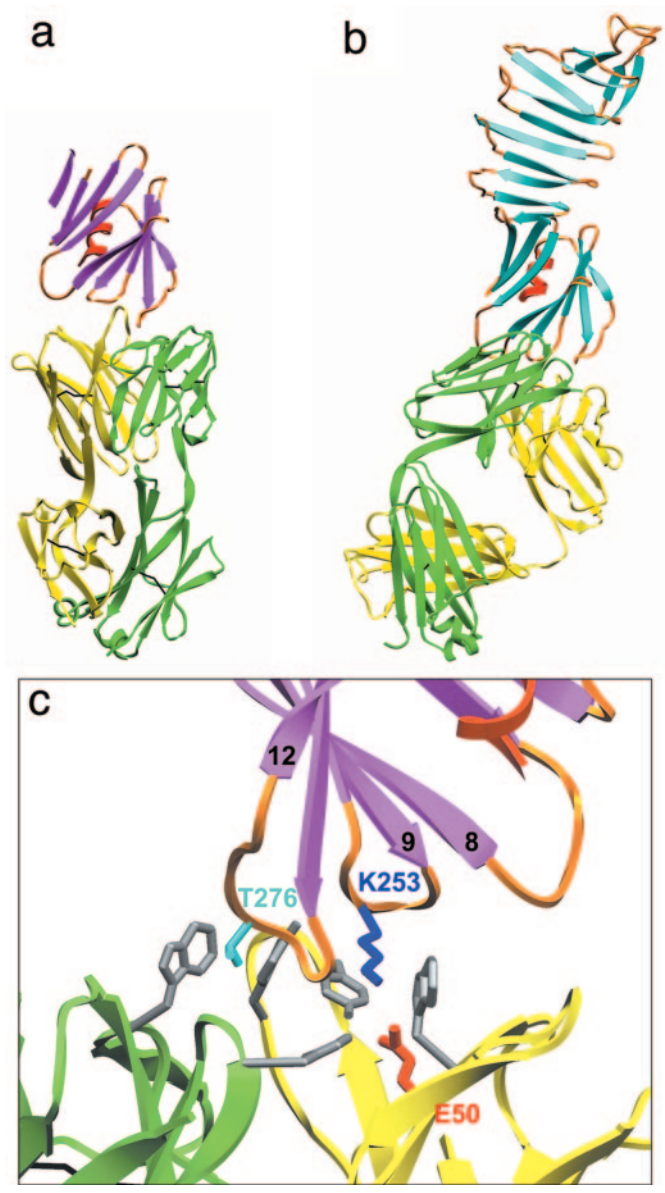

FIG. 3. *a*, *ribbon diagram* of the OspB-CT·H6831 complex. The Fab light chain is in *green*; the heavy chain is in *yellow*. *b*, *ribbon diagram* of the OspA·LA-2 complex, with OspA in approximately the same orientation as OspB-CT (PDB ID 2OSP, Ref. 7). *c*, OspB-CT·H6831 interface. The view is rotated 180 degrees along the vertical axis relative to *a*. Side chains of OspB residues Lys-253 (*blue*) and Thr-276 (*cyan*) are shown along with side chains of Fab aromatic residues (*gray*) and Glu-50 of the H chain (*red*).

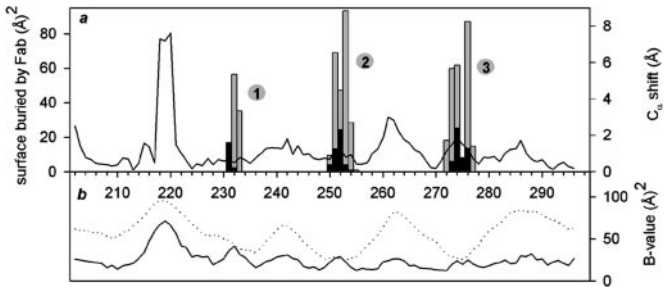

FIG. 4. *a*, superimposed graphs of buried surface area of OspB-CT in the H6831 Fab complex (*bars*, in Å^2) and distances between equivalent OspB-CT Cα-atom positions after least-squares fit of free and Fab-bound structures (*line*, in Å), both plotted *versus* residue number. *b*, main-chain B factors (Å^2) of OspB-CT alone (*solid line*) and OspB-CT in the H6831 Fab complex (*dotted line*) plotted *versus* residue number.

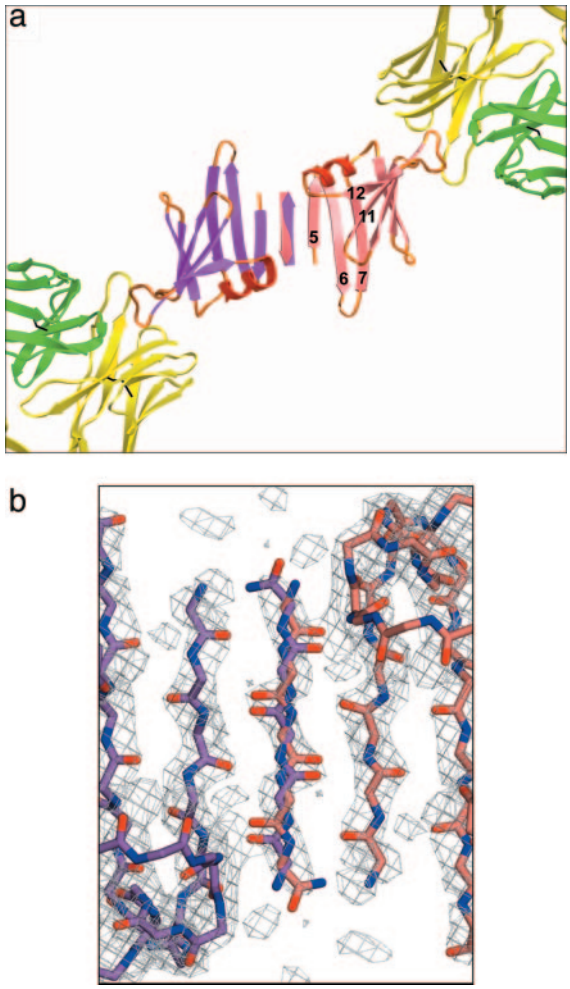

FIG. 5. *a*, *ribbon diagram* of the crystallographic OspB-CT dimer in the OspB-CT·H6831 complex. The extra β-strand connecting the two OspB-CT subunits is shown in both of its possible orientations. *b*, close-up of the region of the crystallographic 2-fold axis. The $2F_o - F_c$, model-phased, sigma-weighted map is shown contoured at 1.0 σ. The 2 populations of polyalanine peptide are modeled in the central density at 50% occupancy. Each provides antiparallel-strand hydrogen bonding to one molecule of OspB, and parallel strand hydrogen bonding to the other.

secondary structure element of the barrel domain. An "extra," apparently unconnected β-strand passes directly through the crystallographic 2-fold and links the two symmetry-related barrels (Fig. 5*b*). The origin of the extra strand is unknown, as the side chains and the polarity of the strand cannot be unambiguously identified. We have modeled the extra strand as a polypeptide of five consecutive alanines with half-occupancy. Application of crystallographic 2-fold symmetry yields two overlapping polypeptides with opposite strand polarity. For each population, the extra strand is parallel to β-strand 5 of one OspB molecule of the crystallographic dimer and is anti-parallel to the other. The position of the extra strand is distinct from that of β-strand 4, the last β-strand of the central sheet in free OspB-CT (Fig. 6, *green strand*).

Comparison of OspB-CT and OspB-CT·Bactericidal Fab Structures—The most striking structural change in OspB-CT between its free and complexed forms is the loss of the first β-sheet, *i.e.* strands 1–4 are not observed in the density. Because the OspB-CT·H6831 complex crystals require several months to grow and are difficult to reproduce, we have not been able to identify the cause. The sheet may simply be grossly disordered, as the missing residues can in principle be accommodated in the adjacent solvent region (total crystal solvent

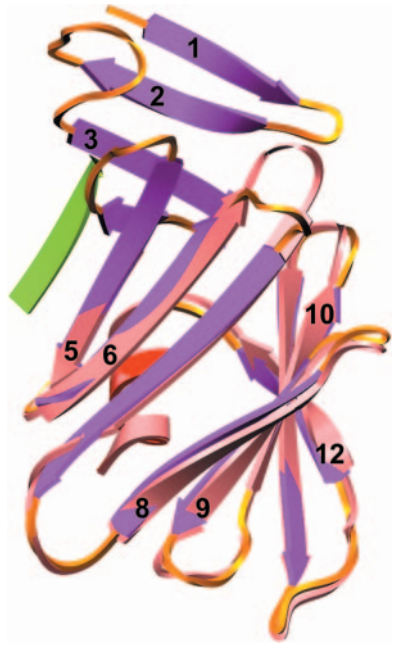

FIG. 6. **Superposition of OspB-CT alone (*violet*) and OspB-CT from the complex (*beige*).** The extra polyalanine β-strand from the complex structure is shown in *green*.

content is 52%). However, this possibility would require two structurally distinct OspB-CT molecules within each crystal artificial dimer: one with the extra β-strand, and one without. A more likely explanation is that the sheet has been proteolytically removed during crystallization, either by a contaminating protease copurified with OspB-CT or H6831 Fab, or possibly by an autoproteolytic activity. In this case all OspB-CT fragments would be considered structurally equivalent, as the extra β-strand would correspond to a completely unconnected polypeptide fragment.

Ding *et al.* (7) found that the C-terminal domain of OspA is essentially unchanged by the binding of LA-2 Fab (r.m.s. deviation of 94 Cα atom positions = 0.46 Å); small positional shifts occur only within residues directly contacted by the Fab. In contrast, the C-terminal domain of OspB-CT exhibits both small positional shifts near the Fab binding site and a few larger structural changes away from the binding site (r.m.s. deviation of 95 Cα atom positions = 1.69 Å; see Fig. 4*a*, *line graph* and Fig. 6). The largest shifts (7–8 Å) correspond to the repositioning of a loop opposite the Fab-binding site (residues 218–220). This loop is poorly ordered in both structures (Fig. 4*b*). In addition, there are modest positional shifts (2–3 Å) at the putative N-terminal residue of OspB-CT in the complex (Thr-202), and in a second non-epitope loop (residues 261–262). In the free OspB-CT structure, all three of these regions are adjacent to the central sheet; in the OspB-CT·H6831 complex they all shift toward, and slightly overlap, the position of the missing sheet. In addition, all three regions with positional shifts are involved in crystal contacts in the complex. These observations suggest that the larger conformational changes are related to the loss of the central sheet, whether through proteolytic cleavage or disorder, and/or to fortuitous crystal contacts. Therefore, the observed conformational changes in OspB-CT may be only indirectly related to Fab binding. Even though the structural differences in OspB before and after complexation seem to be satisfactorily explained by antigen-antibody interactions and crystal-packing interactions, we cannot rule out the possibility that pH differences may also contribute.

DISCUSSION

OspB Structure—The crystal structures we present here confirm that the fold of the C-terminal half of *Borrelia burgdorferi* OspB is identical to that of OspA. We expect that the first four antiparallel β-strands observed in the free OspB-CT fragment correspond in full-length OspB to the C-terminal-half of a free-standing central β-sheet, where the sheet is solvent-exposed on both faces rather than as part of a globular domain. NMR studies indicate that the central β-sheet of OspA is as stable as the center of a more globular fold, even though it is exposed to solvent on both sides (38). OspB-CT antiparallel β-strands 5–7 and 8–12 form two sheets that fold, along with the final α-helix, into the C-terminal barrel domain. The barrel domain of the OspA/B fold features a prominent cleft, with a strictly conserved RE(K/R) trio of partially buried charged residues lying at the base, and an adjacent small cavity lined with strongly conserved hydrophobic residues. This striking arrangement of features, when first observed in OspA, lead us to propose that the C-terminal domain could be a binding site for a small peptide, linear saccharide, or an exposed protein loop (6). Several lines of evidence now suggest that OspA and OspB may be tick-midgut adhesins (11, 39–41), although precise molecular targets have not yet been identified. For OspA, it has been suggested that binding activity to a protease-sensitive factor in tick midgut extract involves the putative binding site residues (39); however, other interpretations of the data are possible (see below). Given the close structural conservation of OspA and OspB, it is likely that the two proteins recognize either the same target, or closely related targets.

OspB has a 23-residue insertion relative to OspA near the N terminus. Since we have been unable to crystallize full-length OspB, the effect of this insertion on the OspA-fold remains unknown. Given its position before the first β-strand of OspA, we have previously suggested that the inserted residues might form an extra pair of β-strands, lengthening the 1st β-sheet from four to six strands (6). However, at least in the context of a recombinant OspB with N-terminal polyhistidine tag in place of the lipid anchor, the inserted region is highly labile to cleavage by certain proteases, which suggests that it may be poorly ordered (42). Structural differences between OspA and OspB N termini could be associated with distinct membrane-associated functions. For instance, OspA, but not OspB, associates with p66, an integral membrane protein with porin activity (43).

OspB Stability and Aggregation—Despite the similarity of the OspA and OspB folds, stability-related properties of these proteins are very different. Both *in vivo* and *in vitro*, OspB is susceptible to cleavage by exogenous proteases, whereas OspA is relatively resistant (16, 42–45). Even without addition of exogenous proteases, recombinant OspB rapidly forms degradation products,[2] whereas recombinant OspA is stable for months to years.

Mutations in OspB appear to further increase sensitivity to proteolysis. C-terminally truncated forms of OspB (apparent molecular mass, 18–21 kDa) are common in intact *B.burgdorferi* (22–24); they appear spontaneously without selection (16, 46), and are enriched after addition of anti-OspB mAbs (32, 33, 47) or after infection of OspB-immunized mice (26). The majority of isolates expressing truncated OspB examined to date have mutations within the C-terminal half of the *ospB* gene leading to premature stop codons (22, 24, 32, 46, 47). In two of six instances, the truncated product is significantly smaller than the predicted size (46, 47). In one isolate producing both full-length and truncated products, the *ospB* gene has several missense mutations, including one likely to disrupt the native fold (Gly-280 → Arg; the main-chain conformation of strictly conserved residue Gly-280 is disallowed for non-glycine residues), but no premature stop (24). These results have raised the possibility that OspB mutants are sensitive to post-translational proteolytic cleavage.

The termination point(s) of all truncated OspB products appear to fall within the residue range 174–201, corresponding to the two C-terminal β-strands of the OspB central sheet (OspB-CT β-strands 3–4). Cleavage of OspB-CT within this residue range also provides a plausible explanation for the structural changes observed in the OspB-CT·H6831 complex structure. The corresponding region of OspA (β12-β13) is more sensitive than neighboring strands to mechanical and thermodynamic unfolding (48–50), and in a truncated OspA expressing only β-strands 1–12, β-strand 12 is disordered (51). The available evidence thus suggests that OspB is even more sensitive than OspA to unfolding in this region.

In the limited proteolysis studies of Katona *et al.* (42), binding of a bactericidal Fab to OspB slowed the relative susceptibility of the N-terminal region of full-length OspB cleavage by added proteases. (These experiments were done over times ranging up to several hours, where OspB remained intact in the absence of added proteases.) This occurred maximally at a stoichiometry of 8–10 mol of OspB per mol of mAb, and the authors considered the case that amyloid-like association of OspB could be taking place, thereby slowing the proteolysis. Amyloid-like fibril formation has been observed with peptides formed from OspA-derived peptides (52), and the promiscuity of β-sheet formation observed in both of the OspB crystal structures described here suggests that this interpretation could be plausible. Similarly, binding of OspA and of short OspA-derived peptides to a protease-sensitive factor in tick gut epithelium was observed to be non-saturating and to include OspA-OspA associations (39); such binding could involve intramolecular β-sheet formation as well.

Recognition by H6831—The OspB-CT·H6831 complex structure provides a satisfactory explanation for the observation that *B. burgdorferi* strains with Thr, Cys, Gly, or Glu in place of Lys at OspB position 253 are resistant to the bactericidal effect of this antibody (30). Given the high complementarity of the interaction observed between H6831 and the OspB Lys-253 side chain, it is unlikely that natural amino acid residues other than Lys could be accommodated at OspB position 253 without loss of binding affinity. Specific substitutions in basic residues of hen egg-white lysozyme (HEL) that are in closely analogous environments in HEL·Fab complexes (Arg-68 → Lys, Lys-96 → Ala, or Lys-97 → Ala) result in 400–10,000-fold losses in binding affinity (53–56).

OspB Lys-253 may represent a "hot-spot" for protective antibody recognition, given its central location with respect to the three adjacent, exposed loops. Two other independently characterized mAbs against OspB, including the bactericidal mAb CB2, are also known to be sensitive to the identity of this residue (32). Reactivity against the topologically equivalent protective LA-2 epitope of OspA is a more reliable indicator of protection against infection from ticks than reactivity against whole OspA antigen (27). The loops recognized by both H6831 and LA-2 are positioned at the end of the antigen opposite the N-terminal lipid anchor, and so are predicted to be highly accessible on the bacterial membrane surface.

Bactericidal Action—Among mAbs directed against *B. burgdorferi* OspA or OspB or against surface proteins of relapsing fever *Borrelia,* several have been shown to trigger cell death without addition of complement or leukocytes (29, 30, 33, 35). The OspA vaccine protects against Lyme disease infection primarily by blocking transmission of *B. burgdorferi* from tick vector to mammalian host during a blood meal (57). Complement-independent killing may play an important role in pre-

venting this transmission, as the complement cascade does not appear to function within the tick (58).

H6831 and, independently, CB2, were the first two mAbs experimentally shown to be bactericidal without complement against *B. burgdorferi*. Cells begin to lyse within minutes after exposure of *B. burgdorferi* culture to either antibody (or corresponding Fab fragment), and viability of the population falls several orders of magnitude over several hours. On a molar basis, Fab fragments of H6831 and a second antibody against *B. hermsii* were found to be as potent as some antibiotics, and the appearance of large numbers of membranous blebs in the presence of these Fabs resembles effects previously observed with cell wall active antibiotics penicillin and vancomycin (30).

The mechanism by which a Fab directly destroys a spirochete appears to represent a novel antibody-organism interaction (31). Two questions we have investigated are whether antibodies that are bactericidal differ from other antibodies, and/or whether the binding of bactericidal Fab affects antigen conformation. We find that the sequence and structure of bactericidal H6831 Fab are typical for the IgG2 heavy chain/kappa light chain class, with no obvious distinguishing features. On the other hand, we do observe structural differences in an OspB antigen fragment between free and H6831-bound forms, although there are several possible causes for these changes, only one of which is Fab binding. It appears that some changes result primarily from proteolysis near the fragment N terminus, and others from changes in crystal packing. It is possible that Fab binding could alter dynamical properties of the OspB fold, which could increase sensitivity to proteolysis or aggregation. Examination of global dynamics of the antigen ± Fab by NMR methods have revealed that the effects of binding can be propagated to regions of the antigen that are distant from the epitope (59, 60).

Whether H6831 affects the conformation or dynamics of OspB, and whether such effects may be important in bactericidal action remains unclear. Since complement-independent bactericidal activity has also been demonstrated for the anti-OspA mAb LA-2,[3] the observation that the structure of OspA is essentially unchanged by LA-2 binding (7) provides additional evidence relevant to the discussion. Considering that bactericidal mAbs appear to target a number of different borrelia antigens (29, 30, 33–35), a specific antigen effect seems unlikely.

A relatively recent discovery is that the Fab portion of all antibodies, regardless of antigenic specificity, catalyze a reaction between singlet oxygen and water, yielding the toxic oxidative species hydrogen peroxide, ozone, and hydroxide radials (reviewed in Ref. 61). The reaction rate is fastest for antibodies with highest UV absorption. It is hypothesized that this activity may represent an ancient mechanism of protection against infection. *B. burgdorferi* may be particularly vulnerable to oxidative damage, as it grows best in environments with limited oxygen, and its genome does not encode a catalase (62). It is attractive to propose that this general property of all antibodies could be the underlying cause. By this mechanism, differences in kinetics or accessibility would explain why some mAbs are bactericidal in the absence of complement, whereas others are not.

In any case, it is puzzling that the bactericidal effect of an Fab against OspB requires the presence of Ca^{2+} (31). This observation indicates that additional factors may be at work.

Possible Autoproteolysis?—The fact that both clonal variants of OspB isolated directly from *B. burgdorferi*, and recombinant OspB overexpressed in the different system of *E. coli*, exhibit truncated OspB forms suggests that proteolysis might be a property intrinsic to the molecule. We find that OspB contains a constellation of residues that resembles the catalytic triad of the serine proteases. These residues are Thr-166, Arg-162, Glu-184; the latter two of which are part of the charged triad of residues adjacent to the putative ligand-binding cleft. Fig. 1*b* shows these residues, as well as possibly influential Arg-214, and the side chain of Asn-164, which forms an H-bond to Thr-166 in the vicinity of the putative oxyanion hole. Also, an alignment with uncomplexed trypsin (PDB ID 1SGT, Ref. 63) is shown in Fig. 7, and detailed interactions are described in the figure legend. As with trypsin, presumably some rearrangement of the loop region would be necessary to form an oxyanion hole during catalysis. Thr and Glu are present in catalytic triads of some members of the broad serine hydrolase family (64), but Arg would seem chemically unlikely to replace His as a general base. However, studies indicate that a Ser-Arg-Asp triad is essential for function in a cytosolic phospholipase A2 (65), and an Arg may function as a catalytic base in an unrelated Sortase A (66). One chemically plausible mechanism for an Arg to function in the catalytic triad of a protease or other enzyme would be for it to facilitate concerted proton transfer, analogous to a "proton wire" (67).

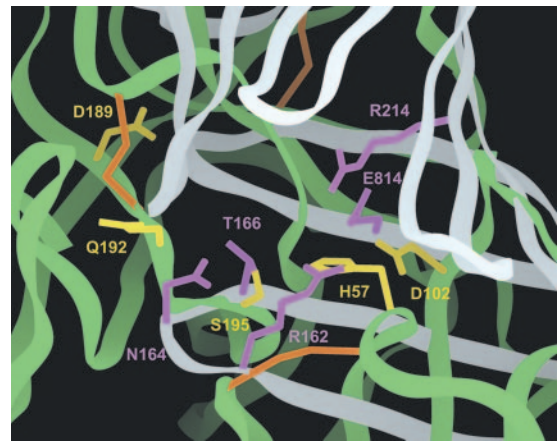

FIG. 7. **Overlay of trypsin (PDB ID 1SGT, *light green*) and of OspB-CT (*white*).** The catalytic triad residues of trypsin (Ser-195, His-57, Asp-102) are shown in *gold*. Disulfide bonds are shown in *brown*. The side chain specificity pocket extends from Ser-195 toward Asp-189 (*gold*); the main chain binding region extends diagonally from Ser-195 toward the *upper right* of the figure. In the substrate/inhibitor-bound forms of trypsin, the oxyanion hole is formed by the side chain of Gln-192 (*gold*), which rearranges, along with backbone amides of Ser-195 and Gly-193 (not shown). Selected OspB-CT residues are shown in *light purple* (see Fig. 1*b* for comparison). Thr-166, Arg-162, and Glu-184 are shown aligned with the catalytic triad of trypsin in a way that gives approximate overlap of open regions of OspB-CT with the side chain specificity pocket and main chain binding region of trypsin. The oxygen atom of the side chain of Asn-164, which is on the loop between β-strands 1 and 2, forms an H-bond with Thr-166. If active in catalysis, this side chain would presumably rearrange to help form the oxyanion hole, along with the backbone amide of Thr-166, and another unidentified coordinating atom.

Acknowledgments—We thank Anya Kycia and Helen Kycia for assistance with crystallization, James Coleman and Jorge Benach for providing a second antibody, CB2, for crystallization trials, and Xiaohua Yang, Benjamin Luft, Dieter Schneider, and Gerard Bricogne for helpful discussions. We also thank Bob Sweet, Malcolm Capel, and Wei Ding for assistance at National Synchrotron Light Source beamlines X12B and X12C, and Helen Berman for providing laboratory space at Rutgers. The Protein Crystallography Research Resource at the NSLS is supported by the Offices of Biological and Environmental Research and of Basic Energy Sciences of the Department of Energy and the National Center for Research Resources of the National Institutes of Health.

REFERENCES

1. Barbour, A. G., and Fish, D. (1993) *Science* **260,** 1610–1616
2. Howe, T. R., Mayer, L. W., and Barbour, A. G. (1985) *Science* **227,** 645–646

[3] X. Yanga and B. J. Luft, manuscript in preparation.

3. Bergstrom, S., Bundoc, V. G., and Barbour, A. G. (1989) *Mol. Microbiol.* **3,** 479–486
4. Brandt, M. E., Riley, B. S., Radolf, J. D., and Norgard, M. V. (1990) *Infect. Immun.* **58,** 983–991
5. Li, H., and Lawson, C. L. (1995) *J. Struct. Biol.* **115,** 335–337
6. Li, H., Dunn, J. J., Luft, B. J., and Lawson, C. L. (1997) *Proc. Natl. Acad. Sci. U. S. A.* **94,** 3584–3589
7. Ding, W., Huang, X., Yang, X., Dunn, J. J., Luft, B. J., Koide, S., and Lawson, C. L. (2000) *J. Mol. Biol.* **302,** 1153–1164
8. Schwan, T. G., Piesman, J., Golde, W. T., Dolan, M. C., and Rosa, P. A. (1995) *Proc. Natl. Acad. Sci. U. S. A.* **92,** 2909–2913
9. Schwan, T. G. (2003) *Biochem. Soc. Trans.* **31,** 108–112
10. Liang, F. T., Caimano, M. J., Radolf, J. D., and Fikrig, E. (2004) *Microb. Pathog.* **37,** 35–40
11. Yang, X. F., Pal, U., Alani, S. M., Fikrig, E., and Norgard, M. V. (2004) *J. Exp. Med.* **199,** 641–648
12. Akin, E., McHugh, G. L., Flavell, R. A., Fikrig, E., and Steere, A. C. (1999) *Infect. Immun.* **67,** 173–181
13. Barbour, A. G., Tessier, S. L., and Hayes, S. F. (1984) *Infect. Immun.* **45,** 94–100
14. Barbour, A. G., Heiland, R. A., and Howe, T. R. (1985) *J. Infect. Dis.* **152,** 478–484
15. Wilske, B., Preac-Mursic, V., Schierz, G., Kuhbeck, R., Barbour, A. G., and Kramer, M. (1988) *Ann. N. Y. Acad. Sci.* **539,** 126–143
16. Bundoc, V. G., and Barbour, A. G. (1989) *Infect. Immun.* **57,** 2733–2741
17. Simon, M. M., Schaible, U. E., Kramer, M. D., Eckerskorn, C., Museteanu, C., Muller-Hermelink, H. K., and Wallich, R. (1991) *J. Infect. Dis.* **164,** 123–132
18. Fikrig, E., Barthold, S. W., Marcantonio, N., Deponte, K., Kantor, F. S., and Flavell, R. A. (1992) *Infect. Immun.* **60,** 657–661
19. Fikrig, E., Telford, S. R., 3rd, Wallich, R., Chen, M., Lobet, Y., Matuschka, F. R., Kimsey, R. B., Kantor, F. S., Barthold, S. W., Spielman, A. and Flavell, R. A. (1995) *J. Exp. Med.* **181,** 215–221
20. Sigal, L. H., Zahradnik, J. M., Lavin, P., Patella, S. J., Bryant, G., Haselby, R., Hilton, E., Kunkel, M., Adler-Klein, D., Doherty, T., Evans, J., and Malawista, S. E. (1998) *N. Engl. J. Med.* **339,** 216–222
21. Steere, A. C., Sikand, V. K., Meurice, F., Parenti, D. L., Fikrig, E., Schoen, R. T., Nowakowski, J., Schmid, C. H., Laukamp, S., Buscarino, C., and Krause, D. S. (1998) *N. Engl. J. Med.* **339,** 209–215
22. Fikrig, E., Tao, H., Kantor, F. S., Barthold, S. W., and Flavell, R. A. (1993) *Proc. Natl. Acad. Sci. U. S. A.* **90,** 4092–4096
23. Schwan, T. G., Schrumpf, M. E., Karstens, R. H., Clover, J. R., Wong, J., Daugherty, M., Struthers, M., and Rosa, P. A. (1993) *J. Clin. Microbiol.* **31,** 3096–3108
24. Probert, W. S., Crawford, M., and LeFebvre, R. B. (1997) *Vaccine* **15,** 15–19
25. Schubach, W. H., Mudri, S., Dattwyler, R. J., and Luft, B. J. (1991) *Infect. Immun.* **59,** 1911–1915
26. Fikrig, E., Tao, H., Barthold, S. W., and Flavell, R. A. (1995) *Infect. Immun.* **63,** 1658–1662
27. Golde, W. T., Piesman, J., Dolan, M. C., Kramer, M., Hauser, P., Lobet, Y., Capiau, C., Desmons, P., Voet, P., Dearwester, D., and Frantz, J. C. (1997) *Infect. Immun.* **65,** 882–889
28. Taylor, P. W. (1992) *Exp. Clin. Immunogenet.* **9,** 48–56
29. Ma, J., Gingrich-Baker, C., Franchi, P. M., Bulger, P., and Coughlin, R. T. (1995) *Infect. Immun.* **63,** 2221–2227
30. Sadziene, A., Jonsson, M., Bergstrom, S., Bright, R. K., Kennedy, R. C., and Barbour, A. G. (1994) *Infect. Immun.* **62,** 2037–2045
31. Escudero, R., Halluska, M. L., Backenson, P. B., Coleman, J. L., and Benach, J. L. (1997) *Infect. Immun.* **65,** 1908–1915
32. Coleman, J. L., Rogers, R. C., Rosa, P. A., and Benach, J. L. (1994) *Infect. Immun.* **62,** 303–307
33. Coleman, J. L., Rogers, R. C., and Benach, J. L. (1992) *Infect. Immun.* **60,** 3098–3104
34. Sadziene, A., Thomas, D. D., and Barbour, A. G. (1995) *Infect. Immun.* **63,** 1573–1580
35. Connolly, S. E., Thanassi, D. G., and Benach, J. L. (2004) *J. Immunol.* **172,** 1191–1197
36. Nicholls, A., Sharp, K. A., and Honig, B. (1991) *Proteins* **11,** 281–296
37. Davies, D. R., and Cohen, G. H. (1996) *Proc. Natl. Acad. Sci. U. S. A.* **93,** 7–12
38. Pham, T. N., Koide, A., and Koide, S. (1998) *Nat. Struct. Biol.* **5,** 115–119
39. Pal, U., de Silva, A. M., Montgomery, R. R., Fish, D., Anguita, J., Anderson, J. F., Lobet, Y., and Fikrig, E. (2000) *J. Clin. Investig.* **106,** 561–569
40. Pal, U., Montgomery, R. R., Lusitani, D., Voet, P., Weynants, V., Malawista, S. E., Lobet, Y., and Fikrig, E. (2001) *J. Immunol.* **166,** 7398–7403
41. Fikrig, E., Pal, U., Chen, M., Anderson, J. F., and Flavell, R. A. (2004) *Infect. Immun.* **72,** 1755–1759
42. Katona, L. I., Ayalew, S., Coleman, J. L., and Benach, J. L. (2000) *J. Immunol.* **164,** 1425–1431
43. Bunikis, J., and Barbour, A. G. (1999) *Infect. Immun.* **67,** 2874–2883
44. Dunn, J. J., Lade, B. N., and Barbour, A. G. (1990) *Protein Expr. Purif.* **1,** 159–168
45. Moroni, A., Sambri, V., Massaria, F., La Placa, M., Jr., Brocchi, E., De Simone, F., and Cevenini, R. (1992) *Microbiologica* **15,** 99–106
46. Rosa, P. A., Schwan, T., and Hogan, D. (1992) *Mol. Microbiol.* **6,** 3031–3040
47. Sadziene, A., Barbour, A. G., Rosa, P. A., and Thomas, D. D. (1993) *Infect. Immun.* **61,** 3590–3596
48. Yan, S., Kennedy, S. D., and Koide, S. (2002) *J. Mol. Biol.* **323,** 363–375
49. Hertadi, R., Gruswitz, F., Silver, L., Koide, A., Koide, S., Arakawa, H., and Ikai, A. (2003) *J. Mol. Biol.* **333,** 993–1002
50. Yan, S., Gawlak, G., Smith, J., Silver, L., Koide, A., and Koide, S. (2004) *J. Mol. Biol.* **338,** 811–825
51. Huang, X., Nakagawa, T., Tamura, A., Link, K., Koide, A., and Koide, S. (2001) *J. Mol. Biol.* **308,** 367–375
52. Ohnishi, S., Koide, A., and Koide, S. (2001) *Protein Sci.* **10,** 2083–2092
53. Sheriff, S., Silverton, E. W., Padlan, E. A., Cohen, G. H., Smith-Gill, S. J., Finzel, B. C., and Davies, D. R. (1987) *Proc. Natl. Acad. Sci. U. S. A.* **84,** 8075–8079
54. Chacko, S., Silverton, E., Kam-Morgan, L., Smith-Gill, S., Cohen, G., and Davies, D. (1995) *J. Mol. Biol.* **245,** 261–274
55. Li, Y., Li, H., Smith-Gill, S. J., and Mariuzza, R. A. (2000) *Biochemistry* **39,** 6296–6309
56. Li, Y., Urrutia, M., Smith-Gill, S. J., and Mariuzza, R. A. (2003) *Biochemistry* **42,** 11–22
57. de Silva, A. M., Telford, S. R., 3rd, Brunet, L. R., Barthold, S. W., and Fikrig, E. (1996) *J. Exp. Med.* **183,** 271–275
58. Rathinavelu, S., Broadwater, A., and de Silva, A. M. (2003) *Infect. Immun.* **71,** 822–829
59. Benjamin, D. C., Williams, D. C., Jr., Smith-Gill, S. J., and Rule, G. S. (1992) *Biochemistry* **31,** 9539–9545
60. Williams, D. C., Jr., Benjamin, D. C., Poljak, R. J., and Rule, G. S. (1996) *J. Mol. Biol.* **257,** 866–876
61. Nieva, J., and Wentworth, P., Jr. (2004) *Trends Biochem. Sci.* **29,** 274–278
62. Fraser, C. M., Casjens, S., Huang, W. M., Sutton, G. G., Clayton, R., Lathigra, R., White, O., Ketchum, K. A., Dodson, R., Hickey, E. K., Gwinn, M., Dougherty, B., Tomb, J. F., Fleischmann, R. D., Richardson, D., Peterson, J., Kerlavage, A. R., Quackenbush, J., Salzberg, S., Hanson, M., van Vugt, R., Palmer, N., Adams, M. D., Gocayne, J., Weidman, J., Utterback, T., Watthey, L., McDonald, L., Artiach, P., Bowman, C., Garland, S., Fujii, C., Cotton, M. D., Horst, K., Roberts, K., Hatch, B., Smith, H. O., and Venter, J. C. (1997) *Nature* **390,** 580–586
63. Read, R. J., and James, M. N. (1988) *J. Mol. Biol.* **200,** 523–551
64. Dodson, G., and Wlodawer, A. (1998) *Trends Biochem. Sci.* **23,** 347–352
65. Pickard, R. T., Chiou, X. G., Strifler, B. A., DeFelippis, M. R., Hyslop, P. A., Tebbe, A. L., Yee, Y. K., Reynolds, L. J., Dennis, E. A., Kramer, R. M., and Sharp, J. D. (1996) *J. Biol. Chem.* **271,** 19225–19231
66. Marraffini, L. A., Ton-That, H., Zong, Y., Narayana, S. V., and Schneewind, O. (2004) *J. Biol. Chem.* **279,** 37763–37770
67. Nagle, J. F., and Morowitz, H. J. (1978) *Proc. Natl. Acad. Sci. U. S. A.* **75,** 298–302
68. Studier, F. W., Rosenberg, A. H., Dunn, J. J., and Dubendorff, J. W. (1990) *Methods Enzymol.* **185,** 60–89
69. Otwinowski, Z., and Minor, W. (1997) in *Methods in Enzymology* (Carter, C. W., and Sweet, R. M., eds) Vol. 276, pp. 307–326, Academic Press, San Diego
70. Navaza, J. (1994) *Acta. Crystallogr. Sect. A* **50,** 157–163
71. Brünger, A. T., Adams, P. D., Clore, G. M., DeLano, W. L., Gros, P., Grosse-Kunstleve, R. W., Jiang, J. S., Kuszewski, J., Nilges, M., Pannu, N. S., Read, R. J., Rice, L. M., Simonson, T., and Warren, G. L. (1998) *Acta Crystallogr. D. Biol. Crystallogr.* **54,** 905–921
72. Lawson, C. L. (1995) *Acta. Crystallogr. Sect. D* **51,** 853–855
73. Murshudov, G. N., Vagin, A. A., and Dodson, E. J. (1997) *Acta Crystallogr. D. Biol. Crystallogr.* **53,** 240–255
74. Laskowski, R. A., MacArthur, M. W., Moss, D. S., and Thornton, J. S. (1993) *J. Appl. Crystallogr.* **26,** 283–291
75. Evans, S. V. (1993) *J. Mol. Graph.* **11,** 134–138

Structural Investigation of *Borrelia burgdorferi* OspB, a BactericidalFab Target

Michael Becker, Jonas Bunikis, Barbara D. Lade, John J. Dunn, Alan G. Barbour and Catherine L. Lawson

J. Biol. Chem. 2005, 280:17363-17370.
doi: 10.1074/jbc.M412842200 originally published online February 15, 2005
